PAPER

Development of skeletal kinetics mechanisms for plasma-assisted combustion via principal component analysis

To cite this article: Aurélie Bellemans et al 2020 Plasma Sources Sci. Technol. 29 025020

View the article online for updates and enhancements.



IOP ebooks™

Bringing together innovative digital publishing with leading authors from the global scientific community.

Start exploring the collection-download the first chapter of every title for free.

Plasma Sources Sci. Technol. 29 (2020) 025020 (14pp)

https://doi.org/10.1088/1361-6595/ab69e6

Development of skeletal kinetics mechanisms for plasma-assisted combustion via principal component analysis

Aurélie Bellemans 10, Nicholas Deak 20 and Fabrizio Bisetti 20

E-mail: aurelie.bellemans@utexas.edu

Received 7 September 2019, revised 28 December 2019 Accepted for publication 9 January 2020 Published 20 February 2020



Abstract

The positive effect of plasma discharges on ignition and flame stability motivates the development of detailed kinetic mechanisms for high-fidelity simulations of plasma-assisted combustion. Because of their hierarchical nature, combustion processes require a large number of chemical species and pathways to describe hydrocarbon oxidation. In order to simulate kinetic enhancement by non-thermal electrons, additional species and processes are included, which model the ionization and excitation of neutral molecules. From a practical perspective, integrating large kinetics mechanisms is computationally burdensome due to the temporal stiffness of the nonlinear combustion dynamics and the memory requirements associated with the high number of species. In order to alleviate computational costs, a dimensionality reduction approach is proposed based on principal component analysis. The methodology is demonstrated on a detailed kinetics mechanism for plasma-assisted combustion excited by a nanosecond pulse discharge. Data are collected from a zero-dimensional two-temperature reactor model, whereby a nanosecond pulse generates a population of excited-state molecules and radicals in argon and air mixtures with hydrocarbon fuels. The data from the detailed mechanism are used to describe the evolution of the plasma and mixture based on principal components. Several skeletal mechanisms consisting of a much smaller number of species are assembled and their accuracy is compared against the detailed one. The performance of selected skeletal mechanisms is found satisfactory for the simulation of plasma-assisted ignition in unsteady, three-dimensional reactive flows.

Supplementary material for this article is available online

Keywords: plasma-assisted combustion, kinetics reduction, principal component analysis, nanosecond pulse discharges

1

1. Introduction

The main physical principle behind the kinetic enhancement of combustion chemistry by plasma discharges is the generation of high-energy, non-thermal electrons that ionize and excite the neutral molecules. As a result, ions, radicals and vibrationally and electronically excited molecules in the non-equilibrium plasma will initiate chain-branching reactions towards the ignition of fuel/air mixtures [1–3]. The electrons lead to the electronic and vibrational excitation of nitrogen and the dissociation of oxygen. Leveraging the internal energy of the species to initiate a chemical reaction proves to

¹ Département d'Aéro-Thermo-Mécanique, Ecole polytechnique de Bruxelles, Université Libre de Bruxelles, Ixelles, Belgium

² Department of Aerospace Engineering and Engineering Mechanics, Cockrell School of Engineering, The University of Texas at Austin, TX 78712

be more efficient than involving thermal energy exchanges only [4, 5].

A primary example is the production of radicals (O, H, OH) through the plasma dissociation of oxidizer and fuel, and quenching of electronic and vibrational states of molecules: a more favorable ignition delay time is obtained for higher initial densities of O and H atoms [6]. Additionally, plasma discharges allow for a thermal effect: the gas temperature increases on short time scales due to ultra-fast heating [7, 8]. This heating is caused by recombination reactions and the relaxation of electronically and vibrationally excited species.

A kinetic mechanism for plasma-enhanced combustion consists of a combination of plasma kinetics with combustion pathways for the simulation of plasma-assisted combustion of hydrocarbon-air mixtures (CH₄ and C₂H₄) [9, 10]. Using a similar strategy, kinetic mechanisms were proposed for the plasma-enhanced combustion of hydrogen-air mixtures [11, 12]. In the most recent mechanisms, special attention was given to the interaction of high-energy electrons with neutral fuel and air species [13, 14]. High-energy electrons create a non-thermal plasma in which the electron temperature is much higher than the temperature of heavy species. Further, the electron energy distribution function is non-Maxwellian and requires the solution of the Boltzmann equation in order to evaluate the electron transport coefficients and rate coefficients. A possible approach to modeling reactions that depend on the electron temperature is to fit the rate coefficients originating from the ab initio calculations to a range of electron temperatures and include them as such in the detailed mechanism. In recent literature [15], this method was adopted to assemble a plasma-assisted combustion mechanism to study the kinetics of plasma-assisted ignition in argon and air. The resulting mechanism was validated by experiments [16-18] and used to study radical production and main reaction pathways in argon and air subject to nanosecond pulse discharges.

Unfortunately, compromises between the accuracy of the mechanism and the computational cost required for its usage need to be made. Because of the large number of species and complex chemical kinetics, zero-and one-dimensional simulations of plasma-assisted combustion using simplified geometries have been performed [19, 20], while large scale threedimensional simulations with detailed plasma and combustion kinetics are uncommon [21]. A strategy to handle plasmaenhanced ignition simulations is to separate the plasma discharge from the ignition calculation. Plasma processes following nanosecond pulsed discharges occur within hundreds of nanoseconds, while ignition and combustion chemistry evolve over milliseconds. It is common practice to first calculate the products of the discharge using a non-equilibrium plasma solver. Once the species distribution at the end of the discharge is calculated, it is used as initial conditions for the combustion simulation [22-24]. Alternatively, a semiempirical model has been proposed to predict nanosecond repetitively pulsed discharge-assisted ignition in turbulent flows [8, 25]. Although this model reflects the non-equilibrium effects on the gas temperature and species concentrations, it does not include detailed non-equilibrium plasma kinetics. The results and physical insight produced by those modeling approaches depends largely on the accuracy of the kinetic mechanism.

Because of the large size of the mechanisms for plasmaassisted combustion and the complex physics they involve, detailed three-dimensional simulations are still out of reach. To overcome this challenge, chemistry reduction techniques may be employed in order to reduce the computational cost. Different strategies are available to reduce the complexity of detailed kinetic mechanisms. In rate-controlled constrained equilibrium theory developed by Keck [26], fast kinetics are projected on the slowly varying modes of the system providing a reduced dynamical representation. This reduced set is obtained by setting constraints, evolving according to the detailed kinetics, whereas fast reactions are assumed to be at equilibrium. In directed relation graph [27], a network of species and reactions is created and analyzed with the aim to keep only a reduced set, which reproduces specified targets, such as species concentration, ignition delay or burning velocity, within a pre-defined accuracy. A possible alternative is offered by lumping techniques. In combustion applications, those techniques regroup species with similar compositions and properties and solve them as one lumped species [28, 29]. For plasma mechanisms, the excited levels in the model are lumped within pseudo-species [30]. Recently, Principal Component Analysis (PCA) has been used to reduce large kinetic mechanisms. PCA is a statistical approach to project a system on a sub-space of lower dimension identified by the principal components. Principal components correspond to the directions with the largest variance in the system. The dimensionality of the system decreases significantly as only a reduced number of variables, the principal components, are solved for [31]. Large combustion mechanisms were reduced using the manifold generated (MG) PCA and score-PCA formulations [32, 33] combined with regression methods [34] and Kriging optimization [35]. For the first time, Peerenboom et al [36] applied PCA to plasma flows in combination with a regression model for the reduction of the vibrational states in CO₂. Previously, MG-PCA [37] and score-PCA [38] were used to reduce kinetics models that describe the ionization of argon shock tubes, leading to a reduction of the number of species in the mechanism by 90%. Score-PCA was combined with a uniform lumping model to reduce the NASA Ames mechanism for N-N2 rovibrational excitation and dissocia-

The objective of the present paper is to adapt reduction approaches based on PCA to plasma-assisted combustion applications. A well-established mechanism available in literature [15] is analyzed and reduced. The present paper is organized as follows. Section 2 explains the reactor model. Section 3 presents the ignition test cases. Section 4 presents the reduction strategy based on PCA. The resulting reduced-order model is presented in section 5 and used to generate a skeletal mechanism. The accuracy of the skeletal mechanisms is also appraised against the detailed one. Conclusions are presented in section 6.

2. Reactor and kinetics model

A zero-dimensional reactor solver is developed in order to investigate plasma-assisted ignition via nanosecond pulse discharges. The reactor model is isochoric and adiabatic, featuring a two-temperature model to describe non-thermal electrons.

2.1. Reactor model

The governing equations describe the time evolution of a closed isochoric, and adiabatic reactor. The plasma is described by two temperatures: T_e for the electrons and T for all other species. Let n_e indicate the number density of electrons and n_i ($i \neq e$) the number density of particles other than electrons. The concentrations evolve according to the following ordinary differential equations

$$\frac{dc_e}{dt} = \omega_e,\tag{1}$$

$$\frac{dc_i}{dt} = \omega_i, \qquad i \neq e \tag{2}$$

with ω_i indicating the molar production rate of species *i*. Let $u_e = u_e(T_e)$ indicate the molar internal energy of the electrons and $u_i = u_i(T)$ that of species *i*. The internal energy densities are therefore $U_e = u_e c_e$ for the electrons and $U_i = u_i c_i$ for the other particles. Consider $c_{v,i}$ as the specific heats at constant volume of each species and $c_{v,e} = 3k_{\rm B}/2$ ($k_{\rm B}$ is the Boltzmann constant) the one of the electrons, we write two evolution equations for the temperature of the electrons and that of all other particles

$$\frac{\mathrm{d}T}{\mathrm{d}t} = \frac{1}{\sum_{i \neq e} c_{v,i} c_i} \left(-\sum_{i \neq e} \omega_i u_i - Q_{\mathrm{el}} - Q_{\mathrm{inexc}} - Q_{\mathrm{loss}} \right), \quad (3)$$

$$\frac{\mathrm{d}T_e}{\mathrm{d}t} = \frac{1}{c_{v_e}c_e}(-\omega_e u_e + Q_{\mathrm{el}} + Q_{\mathrm{inexc}} + Q_{\mathrm{loss}} + Q_E). \quad (4)$$

The source terms $Q_{\rm loss}$, $Q_{\rm inexc}$ and $Q_{\rm el}$ (SI units: J m⁻³ s⁻¹) describe the energy exchange between the electrons and all other species. A negative source terms implies the energy is lost by the electrons. Those source terms are calculated by evaluating the rate of progress q_r (SI units: mol m⁻³ s⁻¹) for every reaction r

$$q_r = k_{fr} \prod_{i=1}^{N_s} c_i^{\nu'_{ir}} - k_{br} \prod_{i=1}^{N_s} c_i^{\nu''_{ir}},$$
 (5)

where N_s is the number of species, ν'_{ir} and ν''_{ir} the stoichiometric coefficients of the reactants and products, respectively, k_{fr} the forward and k_{br} the backward rate coefficients of the rth reaction. Those contributions are summed together according to the class of energy exchange (i.e. recombination, ionization, excitation, and elastic exchanges) as follows:

• $Q_{\rm loss}$ describes the energy lost by the electrons through recombination processes

$$Q_{\text{loss}} = \sum_{r \in K} - u_e N_{\text{A}} q_r, \tag{6}$$

with K the ensemble of recombination reactions, u_e (SI

units: J) the internal energy of the electrons, N_A the Avogadro number.

• Q_{inexc} is the inelastic energy exchanged due to ionization and excitation processes

$$Q_{\text{inexc}} = \sum_{r \in I} -E_{\text{exc}} N_{\text{A}} q_r, \tag{7}$$

with L the ensemble of ionization and excitation reactions, $E_{\rm exc}$ the excitation or ionization energy and r an excitation reaction. $E_{\rm exc}$ describes the energy increase/decrease when a species is excited from its ground state/excited level to another excited level. For a ionization reaction, $E_{\rm exc}$ represents the ionization energy.

 \bullet $Q_{\rm el}$ describes the elastic energy exchanges

$$Q_{\rm el} = \sum_{r \in M} \sum_{i \in S} -3N_{\rm A} \frac{m_e}{m_i} k_{\rm B} (T_e - T) c_i c_e k_{fr}.$$
 (8)

The expression $3m_e/m_i k_{\rm B}(T_e-T)$ describes the energy lost in one elastic collision. Note that this expression uses the forward rate coefficient k_{fr} and not the rate of progress q_r .

• The power deposited by the discharge per unit volume, Q_E , is modeled as a source term in the electron temperature equation according to a Gaussian pulse

$$Q_E(t) = \frac{E}{\sigma\sqrt{2\pi}} \exp\left(-\frac{1}{2} \frac{(t-\mu)^2}{\sigma^2}\right),\tag{9}$$

with μ the time of peak power, σ the pulse width related to the full-width-half-max FWHM = $2\sqrt{2\ln 2\sigma}\approx 2.355\sigma$, and E the energy density of the pulse. These parameters are chosen to approximate the plasma discharge observed in the experiments. The discharge consists of one pulse or a sequence of pulses with a pulse frequency f.

Equations (1)–(4) are integrated with the stiff solver CVODE available in the SUNDIALS suite [40].

2.2. Kinetic mechanism

The present work uses two mechanisms by Adamovich et al [14]. The first mechanism considered is a fuel-oxygen mechanism with argon diluent (C_rH_v-O₂-Ar). It is common practice to dilute the fuel-oxygen mixture in a neutral gas such as argon, nitrogen or helium when studying kinetics (e.g. pyrolysis and oxidation) at constant temperatures and pressures. The mechanism includes pathways for the combustion of three fuels: methane (CH₄), ethylene (C₂H₄) and propane (C₃H₈), using 103 species and 876 reactions. Among these 876 reactions, 30 depend solely on the electron temperature T_e . The mechanism incorporates electron impact rate coefficients for excitation and ionization reactions with Ar, O2, O, CH_4 , C_2H_4 and C_2H_2 . The rates for the quenching of Ar^* by CH₄, C₂H₆ and C₂H₄ were taken from the literature [41, 42]. In total, 4 ions are included: O_2^+ , H_2^+ , Ar^+ , and Ar^{2+} . The vibrational excitation of O_2 is neglected.

The second kinetics mechanism is specific to air and includes pathways for the same three fuels (methane, ethylene, and propane) using 163 species and 1167 reactions, of

Table 1. Various ignition test cases are considered in this work. Case (a) is the ignition of propane in diluted argon using a single pulse. Case (b) is the ignition of ethylene in air using a single pulse. Case (c) is the ignition of ethylene in air using a burst of identical pulses.

	Case (a)	Case (b)	Case (c)
Gas	Argon	Air	Air
Temperature (K)	750	800	800
Pressure (atm)	1	0.5	0.5
Fuel	C_3H_8	C_2H_4	C_2H_4
Equivalence ratio	1	1	1
Power source type	Single	Single	Burst
Peak power density (kW cm ⁻³)	30	2000	2000
FWHM (ns)	5	15	15
Pulse burst frequency (kHz)	_	_	100
Ignition delay time (μ s)		_	39

which 79 depend on the electron temperature. The same electron impact rate coefficients are included with the addition of supplementary dissociation and excitation reactions for the hydrocarbons. Additional electron impact rate coefficients are provided for N_2 , H_2 and C_3H_8 . The vibrational excitation of O_2 is neglected, but 8 vibrationally excited N_2 species are included. The molar concentrations of hydrocarbons are very small, so that O_2 and N_2 , which together account for about 93% volume, are mostly responsible for generating ions/ electrons. Therefore, only O_2^+ and N_2^+ are included in the model.

For both mechanisms, we have refitted all electron impact rate coefficients starting from data obtained from the Boltzmann equation solver, Bolsig+ [43] using the most recent cross sections in the LxCat database [44]. Electron–electron momentum effects were neglected. The rotational excitation of the molecules was neglected. The rate coefficients were tabulated over an electron temperature range of $0.1-100 \, \text{eV}$, using a composition of $20\% \, \text{O}_2$ and $80\% \, \text{N}_2$.

3. Ignition simulations

The argon and air mechanisms are used to simulate various ignition test cases as detailed in table 1. Case (a) features ignition of propane in diluted argon using a single nanosecond pulse. The reactor and power settings were selected according to the flow reactor experiments described by Eckert *et al* [15]. Cases (b) and (c) consist of the ignition of ethylene in air using a single pulse and a burst of pulses, respectively. The power of the discharge was chosen in order to obtain mixture ignition within the order of $40~\mu s$ of the first discharge pulse.

Figure 1 shows the time evolution of the species number densities of Ar*, O, H, OH, O(¹D) and electrons during a single pulse discharge in a C₃H₈–O₂-argon mixture using 553 ppm of fuel (see Case (a) in table 1). Important radicals such as O, H and OH are produced together with excited oxygen and argon. After a number of pulses, the concentration of carbon dioxide increases abruptly, signaling that conventional exothermic reactions responsible for most of the

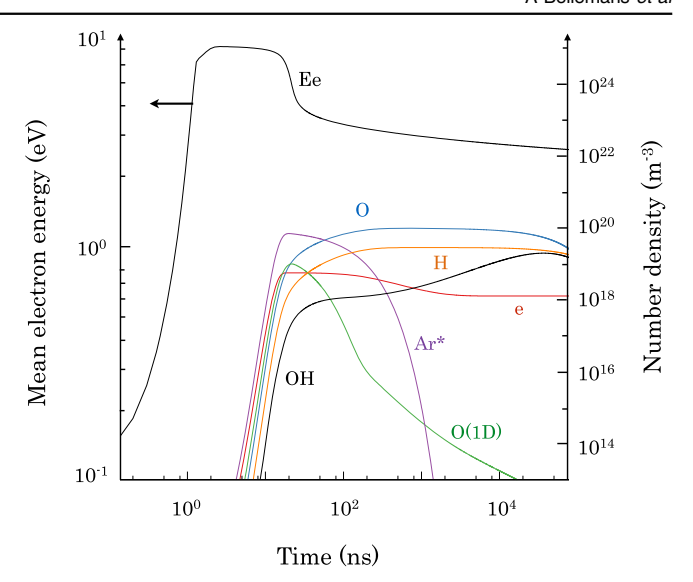


Figure 1. A single discharge in a C₃H₈–O₂–Ar mixture at 750 K and 1 atm produces air radicals (O, H, OH) and excited argon (Ar*) and oxygen (O(¹D)).

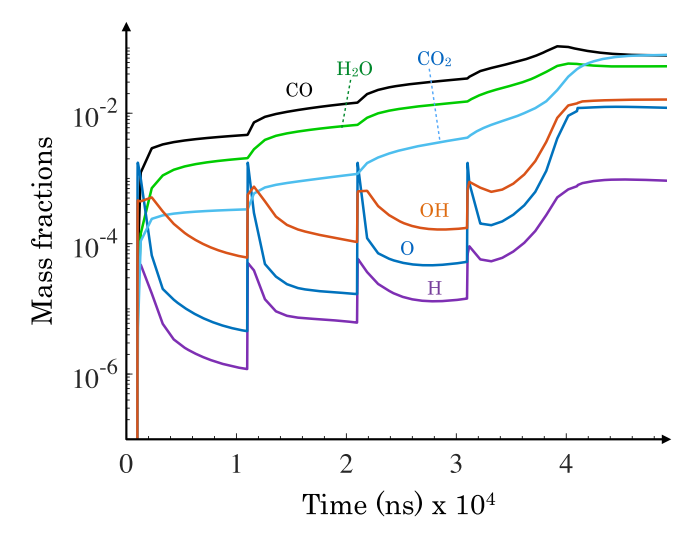


Figure 2. A burst of pulses produces a sustained amount of species and radicals as shown here for a C_2H_4 -air mixture at 800 K and 0.5 atm.

heat release rate undergo a rapid acceleration consistent with an ignition event. Thus, the instant in time when the rate of change in the number density of CO_2 is maximum, is taken to represent the time of ignition t_0 . Then, the time to ignition is defined as $TTI = t_0 - t_1$, where t_1 is the timing of the peak discharge power during the first pulse. Thus, the TTI represents the interval between the first pulse and ignition.

The ignition of ethylene using a burst of identical pulses (see Case (c) in table 1) is shown in figure 2. A burst of pulses produces a sustained amount of radicals as confirmed by the increase of O, H and OH with every pulse. The fuel is fragmented leading to combustion products CO, CO₂ and H₂O. The mixture ignites after 4 pulses at \approx 40 μ s. Figure 3 shows how much of the total power generated by the discharge (Q_E) is transferred to ionization, and electronic and vibrational

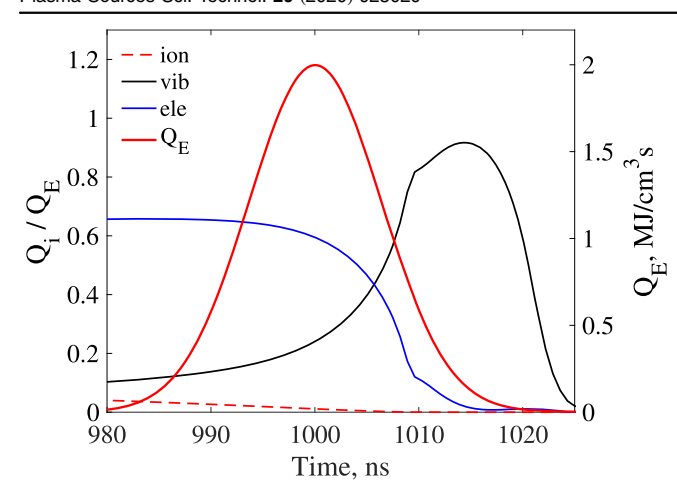


Figure 3. The power deposited by the discharge (Q_E) is used to generate ions, and electronically and vibrationally excited states in C_2H_4 -air mixture at 800 K and 0.5 atm.

excitation reactions. During the discharge itself, the power mainly goes to the excitation of electronically excited states.

4. Mechanism reduction

As demonstrated in recent studies [39], PCA is an effective method to reduce the dimensionality of large kinetic mechanisms by projecting a detailed system consisting of Q variables on a smaller, approximate set with only q < Q principal components. The computational cost decreases considerably as only a subset of the original variables, the principal components, are solved for.

Training data are collected from simulations performed with the detailed mechanism. The data contain the value of all variables for each observation. The variables correspond to the molar concentrations of the species in the mechanism. The sample data are organized in matrix \mathbf{C} , of size $[n \times Q]$ with n the number of observations or points in space or time

$$\mathbf{C} = \begin{bmatrix} c_{11} & \dots & c_{1Q} \\ \vdots & \ddots & \vdots \\ c_{n1} & \dots & c_{nQ} \end{bmatrix}. \tag{10}$$

In order to prepare the data, outliers are removed and the data are scaled and centered using pre-processing techniques. Outliers are those observations that are either very large or very small in magnitude compared to the others. The scaling operation is essential as the magnitude of the variables in the training set varies over several orders of magnitude. In order to capture the variance within the system, it is essential that all variables are expressed on a normalized scale. An overview of various scaling techniques for chemically reactive systems is given by Parente *et al* [45]. The selection of an optimal scaling method is addressed in the results section.

In order to obtain the principal components, an eigenvalue problem is solved for the covariance matrix S using observed data. The matrix of the right eigenvectors A, resulting from the largest eigenvalues L, correspond to the principal components, also called scores, in the reduced

representation

$$\mathbf{S} = \frac{1}{n-1} \mathbf{C}^T \mathbf{C} = \mathbf{A} \mathbf{L} \mathbf{A}^T. \tag{11}$$

The matrix of eigenvectors is truncated to a matrix \mathbf{A}_q containing only the q < Q eigenvectors corresponding to the highest eigenvalues or variance as described in Sutherland et al [45]

$$\mathbf{Z}_q = \mathbf{C}\mathbf{A}_q,\tag{12}$$

$$\tilde{\mathbf{C}}_q = \mathbf{Z}_q \mathbf{A}_q^T. \tag{13}$$

The principal components are a linear combination of the original variables. When inverting equation (12), one recovers the original data as shown in equation (13). The scores do not relate to the original space given by the conserved variables, which are in this case the molar concentrations, but do relate to the eigenvectors of the variables. The governing equations must be solved in this space and should be rewritten accordingly. Additionally, the species source terms are transformed to the space of principal components by using the truncated matrix of eigenvectors $\mathbf{A}_{\mathbf{G}}$:

$$\omega_Z = \omega_C \mathbf{A_q}. \tag{14}$$

Practically, a matrix-vector multiplication is performed every iteration in order to retrieve the concentrations of all species. This cost of the operation is negligible with respect to the computational cost of solving the ODEs in the first place.

PCA can also be used as a tool to interpret the evolution of a complex system of large dimensionality. The principal components or scores are a linear combination of the original variables

$$\mathbf{z} = \sum_{i=1}^{Q} b_{ij} c_j, \qquad i \in \{1, ..., q\}$$
 (15)

with \mathbf{z} indicating a score or principal component and \mathbf{c} the vector containing the original variables, in this case the molar concentrations of the species. The weights or loadings, denoted by b_{ij} , are chosen to maximize the variance within the data. Analyzing these loadings for all scores, which are contained in the matrix A_q , provides insight into the problem. The varimax rotation method is applied on the matrix of eigenvectors in order to maximize the information contained in the weighting factors as demonstrated in previous work [46].

5. Discussion

The objective of this work is to obtain a reduced-order representation of a detailed plasma-combustion chemical kinetics mechanism using PCA. The reduced model obtained from the analysis is then used to investigate plasma-enhanced combustion kinetics. The strategy is as follows: data are collected from the zero-dimensional simulations and used for PCA. The data are sampled across the entire simulation in order to capture changes in composition. The first step in the analysis is to develop a model *a priori*. Once reduced models

Table 2. Scaling techniques for data pre-processing.

Scaling technique	Scaling variable		
Auto (std)	s (standard deviation)		
Level	$\bar{\mathbf{c}}$ (mean value)		
Range	$\max(\mathbf{c}) - \min(\mathbf{c})$		
Max	$\max(\mathbf{c})$		
Pareto	\sqrt{s}		
VAriable STability (vast)	$s^2/\bar{\mathbf{c}}$		

are identified, their performance is verified *a posteriori* with new simulations. A complete analysis is carried out on Case (a) in table 1, which consists of nanosecond discharges in a propane-air mixture diluted with argon. The methodology is thereafter applied to simulate the ignition of an ethylene/air mixture in low pressure using a burst of nanosecond pulse discharges as in Case (c) in table 1.

5.1. Nanosecond pulse discharges in argon

5.1.1. A priori analysis. Zero-dimensional reactor simulations with the detailed $Ar-O_2-C_3H_8$ mechanism are performed. The mixture consists of 553 ppm of fuel and 3000 ppm of O_2 with balancing argon at 1 atm and 750 K. The mixture is excited by a single pulse with a pulse FWHM equal to 5 ns and a peak power density of $30 \, \text{kW cm}^{-3}$.

The first step towards a PCA-based reduced model is the preprocessing of the data: outlying data points are removed and the data are centered and scaled. In order to detect outliers, the distance of each state vector with respect to the data center is computed with the Mahalanobis distance [47]

$$D_M = (\mathbf{C} - \bar{\mathbf{C}})^T \mathbf{S}^{-1} (\mathbf{C} - \bar{\mathbf{C}}), \tag{16}$$

with matrix $\bar{\mathbf{C}}$ a matrix containing the average values of the variables. Observations for with a large D_M are discarded from the set. Various scaling methods are compared towards an optimal preprocessing of the data. The required amount of principal components is retained using a scree plot and simulations whereby a subset of the principal components is used are performed and compared against the detailed model.

The centering operation centers the data for each variable, in our case each species molar concentration \mathbf{c} , by subtracting its average value $\bar{\mathbf{c}}$

$$\mathbf{c}_{\text{centered}} = \mathbf{c} - \bar{\mathbf{c}}.$$
 (17)

The centered data is scaled using a scaling variable s from one of the methods described in table 2

$$\mathbf{c}_{\text{scaled}} = \mathbf{c}_{\text{centered}}/s.$$
 (18)

In order to determine the most suitable technique, the methods are compared by calculating the R^2 error of the reconstructed variable after PCA for a decreasing number of principal components as shown in figure 4. The error is estimated as follows

$$R^{2} = \frac{\sum (\tilde{\mathbf{c}} - \bar{\mathbf{c}})^{2}}{\sum (\mathbf{c} - \bar{\mathbf{c}})^{2}},$$
(19)

with $\tilde{\mathbf{c}}$ representing the reconstructed variables and $\bar{\mathbf{c}}$ the average value of the variable. Figure 4 compares the standard, Pareto, level and max scaling methods for the reconstruction of H_2O , O, C_3H_8 and OH. The best scaling technique for the reconstruction of the major species H_2O , O and C_3H_8 is the Pareto scaling method as the R^2 remains the closest to 1 for a small retention of principal components. Up to 3 principal components, level scaling remains the best method for the reconstruction of the radicals. From the latter analysis it can be concluded that all scaling methods perform similarly up to a small number of principal components. Pareto scaling shows promising results for most of the species molar concentrations analyzed.

The main objective of PCA is to identify the smallest set of principal components that provide an accurate reduced representation of the full system. An indication of the dimensionality of the set is given by a scree graph. A scree graph plots the eigenvalue magnitude against its index. From such a plot, a break between small and large eigenvalues becomes apparent, guiding the selection of an optimal number of variables q. Figure 5 shows the scree graph for various scaling techniques. Based on the normalized eigenvalues obtained with max scaling, we observe a break after 25 principal components. Similar results are obtained with level scaling. Using standard scaling, the number of retained components increases to 30. No natural break is observed using Pareto scaling. Therefore, we conclude that the optimum amount of principal components is around 25. This result suggests the potential for a model compression from 103 to 25 variables or 76%.

A reduced-order representation of the detailed chemistry is obtained using 25 principal components (q = 25). By definition, a principal component is a linear combination of the molar concentrations of all species, thus the data in figures 6 and 7 show the relative contribution of each species to select principal components. A negative weight means that the species has a negative coefficient in the principal component. Figure 6 shows the weights for the first 4 principal components in a reduced model with q = 25. The first principal component (PC1 in figure 6(a)) shows major contributions from $O_2(a^1\Delta)$, C_3H_8 , C_3H_6 , C_2H_4 and H_2O . Those species relate directly to the fuel-air plasma reactions involving the oxygen metastable $O_2(a^1\Delta)$. The importance of $O_2(a^1\Delta)$ in oxygen discharges has been demonstrated in previous work by Franklin [48]. The oxygen metastable species is known to have a low destruction rate and is longlived. The species C₃H₈, C₃H₆, C₂H₄ and H₂O show the process of oxidation of the fuel and its break-down into smaller hydrocarbons. Moreover, PC1 shows important contributions for the species nC₃H₇ and iC₃H₇, which can be traced back to the following reactions

$$C_3H_8 + O_2 \leftrightharpoons nC_3H_7 + HO_2,$$
 (20)

$$C_3H_8 + O_2 = iC_3H_7 + HO_2,$$
 (21)

$$C_3H_8 + HO_2 \leftrightharpoons nC_3H_7 + H_2O_2,$$
 (22)

$$C_3H_8 + HO_2 = iC_3H_7 + H_2O_2,$$
 (23)

$$C_3H_8 + OH \leftrightharpoons nC_3H_7 + H_2O, \tag{24}$$

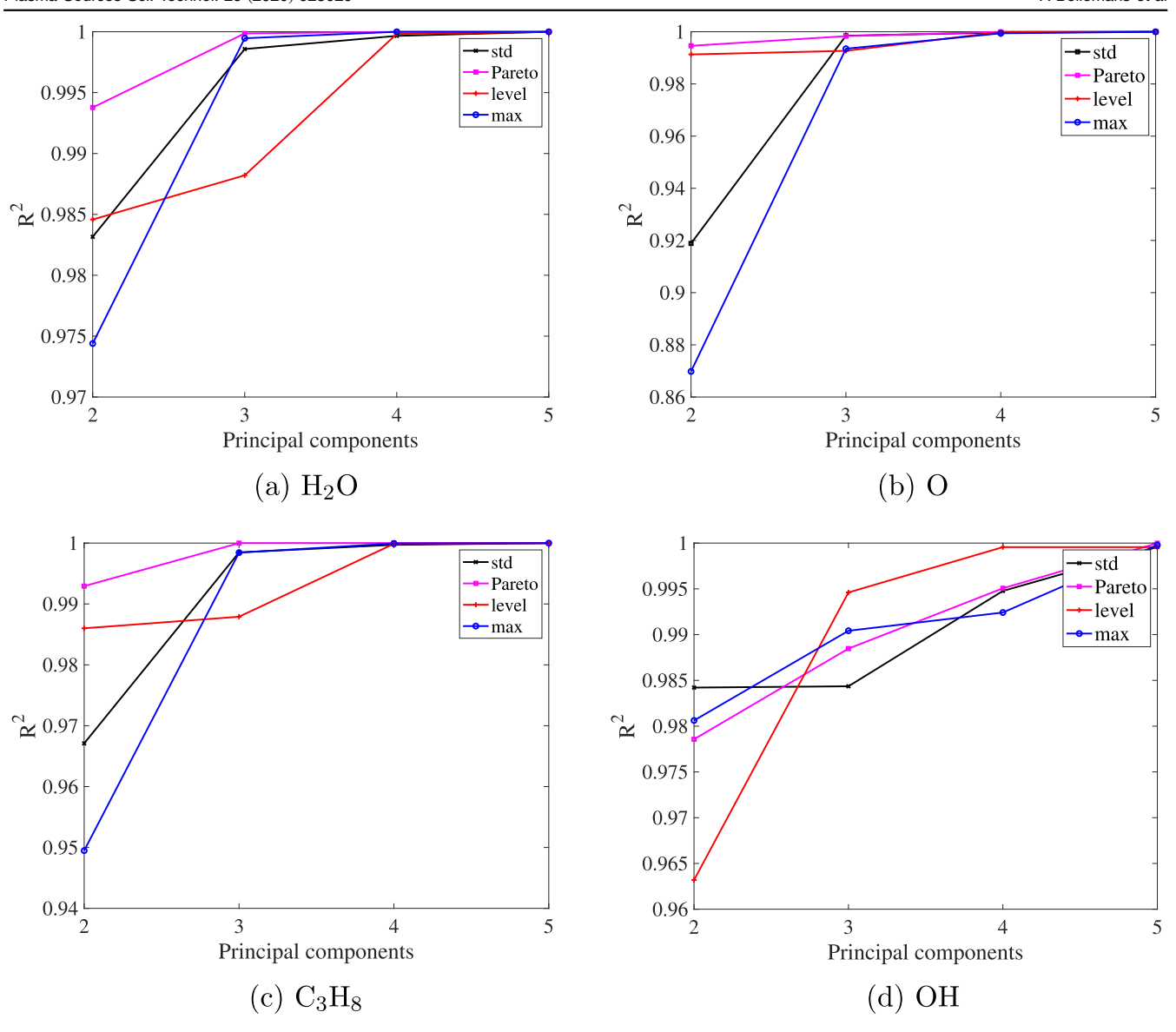


Figure 4. Comparison of the standard, max, level, and Pareto scaling methods for the reconstruction of molar concentrations for Case (a). R^2 error as a function of the number of principal components.

$$C_3H_8 + OH = iC_3H_7 + H_2O,$$
 (25)

$$C_3H_8 + O \leftrightharpoons nC_3H_7 + OH, \tag{26}$$

$$C_3H_8 + O = iC_3H_7 + OH, \qquad (27)$$

$$C_3H_8 + H \leftrightharpoons nC_3H_7 + H_2, \tag{28}$$

$$C_3H_8 + H = iC_3H_7 + H_2,$$
 (29)

$$C_3H_8 + C_2H_5 \leftrightharpoons nC_3H_7 + C_2H_6,$$
 (30)

$$C_3H_8 + C_2H_5 \leftrightharpoons iC_3H_7 + C_2H_6,$$
 (31)

$$C_3H_8 + C_2H_5 \rightarrow RC_3H_7 + C_2H_6,$$
 (31
 $C_3H_8 + iC_3H_7 \Rightarrow nC_3H_7 + C_3H_8,$ (32

$$\mathbf{T}(\mathbf{H} + \mathbf{O} + \mathbf{C}\mathbf{H} + \mathbf{H}\mathbf{O}) \tag{22}$$

$$nC_3H_7 + O_2 \leftrightharpoons C_3H_6 + HO_2. \tag{33}$$

The latter species and reactions do also appear in principal components 2, 3 and 4 as shown in figure 6, and constitute the core of the mechanism describing plasmaassisted combustion of the C₃H₈–O₂–Ar mixture.

The main dynamics in a plasma-assisted combustion problem consists of (1) the production of primary radicals and

(2) the oxidation of the fuel. The production of radicals occurs during the energy deposition by the discharge. In order to explore this process, the PCA was repeated including samples from the first 20 ns only, when the discharge takes place. Most of the variance, 93%, is carried by the first principal component. This implies that one principal component allows retrieving the full dynamics of the chemistry during the discharge. Figure 7 shows the weights attributed to the original species in the first principal component. This component clearly reflects the production of the O radical and excited species Ar^* , $O(^1D)$ and $O_2(a^1\Delta)$. The most important excited species is the excited state Ar*, which is created by the electron impact reaction and consumed by quenching

$$e^- + Ar = Ar^* + e^-, \tag{34}$$

$$Ar^* + Ar \leftrightharpoons Ar + Ar,$$
 (35)

$$Ar^* + Ar + Ar = Ar + Ar + Ar.$$
 (36)

(32)

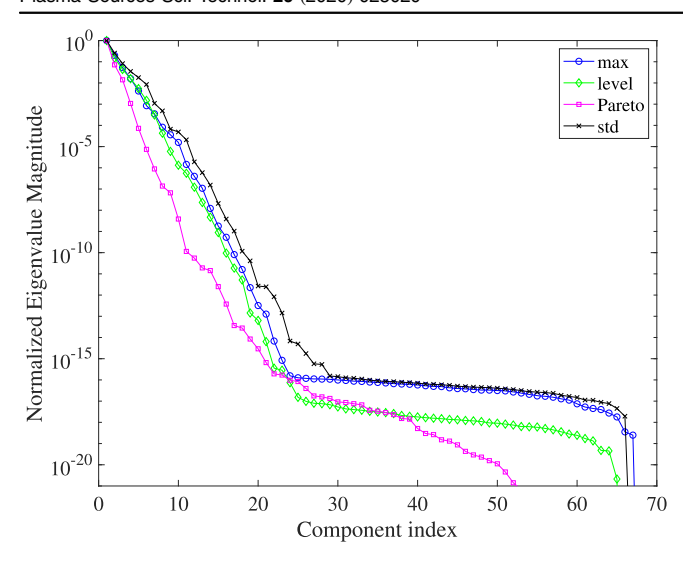


Figure 5. The scree plot shows the normalized eigenvalues against the principal component index for various scaling methods for case (a). When using Pareto scaling, the detailed model can be approximated using 25 principal components.

Other reactions are the electron impact dissociation of oxygen

$$e^- + O_2 = O + O(1D) + e^-,$$
 (37)

$$e^- + O_2 = 2O(1D) + e^-.$$
 (38)

Ions are produced through the following ionization reaction

$$e^- + Ar \leftrightharpoons Ar^+ + 2e^-, \tag{39}$$

$$e^- + O_2 = O_2^+ + 2e^-.$$
 (40)

Small quantities of the oxygen metastable $O_2(a^1\Delta)$ are created via electron impact excitation

$$e^- + O_2 \leftrightharpoons O_2(a^1 \Delta) + e^-. \tag{41}$$

The de-excitation of the metastable form of argon results in the break-up of propane into propene as follows

$$Ar^* + C_3H_8 = Ar + C_3H_6 + 2H.$$
 (42)

These findings are consistent with the conclusions reported recently in the literature [15].

5.1.2. A posteriori analysis. The previously derived model has been used in the reactor code in order to verify its reliability and accuracy. In order to solve for principal components, a change of basis must be performed to transform the variables from the molar masses to the space spanned by the principal components using the matrix relation as shown in equation (12). This procedure applies to both species and source terms The correct implementation of the PCA method in the code has been verified by retaining all species as principal components and verifying that the original states are reconstructed without error.

The *a priori* analysis on the species molar concentrations showed that about 25 principal components allow for a perfect reconstruction of temporal evolution of the mixture. However, the size of the state-space has been determined *a priori*, and might vary once the evolution of the mixture is

described by the evolution of a subset of the principal components only. The number of principal components in the model was lowered from 103 (i.e. the full size of the system). In order to verify the performance of the reduced model, the reconstructed species are computed and compared against the reference solution. A minimum was found for a PCA-based reduction based on 21 principal components. This implies that the size of the mechanism was reduced by 80%. Figure 8 represents the time evolution of the main radicals for the PCA-based reduced model against the full model. An accurate reconstruction has been obtained ($R^2 = 0.95$ over the entire simulation).

Figure 9 shows the time evolution of the principal components using the reduced-order model with 21 components. Principal components 1 (see figure 6(a)), 2 (see figure 6(b) and 4 (see figure 6(d)) control the evolution of the system. Component 3 plays a major role during the discharge phase over a time scale of a few nanoseconds, while components 1 and 2 track the global variation of the mixture after the discharge.

The reduced model was trained on data from Case (a) corresponding to plasma reactor experiments at 1 atm and an initial temperature of 750 K. The accuracy of the model was demonstrated by comparisons against data with the detailed mechanism. Despite this success, it is important to asses whether the model is accurate for conditions other than those used for its training. Next, the input temperature is varied from 750 to 1250 K. All flow reactor experiments were performed at 1 atm. Using the model with 21 components, results are inaccurate if the initial temperature changed with respect to the value used during training. Increasing or decreasing the inlet temperature resulted in large discrepancies in the species molar concentrations. However, adding principal components to the reduced model solved this issue. A PCA-based model using 40 principal components reproduced the reactor kinetics up to a maximum temperature of 1250 K. Table 3 shows the R^2 error for the reconstruction of the molar concentrations of O, OH, H and H₂O using 40 principal components. Increasing the temperature from 750 to 1250 K resulted in a good agreement with a $R^2 = 0.9878$ for O. The R^2 shows discrepancies for H_2O after 1050 K. Unfortunately, decreasing the temperature under 750 K did not give any satisfactory results. From this investigation we can conclude that the low-temperature simulations need a different PCA-based model based on data obtained with lower temperatures. The species that are represented in the first principal components for the 750 K case are not suitable to represent plasma-assisted ignition at lower temperatures. Possible remedies to this issue are: the training the PCA with a broader set of inlet temperatures; and allowing a larger number of principal components.

5.2. Nanosecond pulse discharges in ethylene/air mixtures

Next, we consider the ignition of ethylene in air at 0.5 atm and 800 K as described in case (b) and (c) in table 1. Initially, 654 ppm of fuel is mixed with air with a small initial concentration of seed electrons (10^{15} m^{-3}) . The mixture is ignited

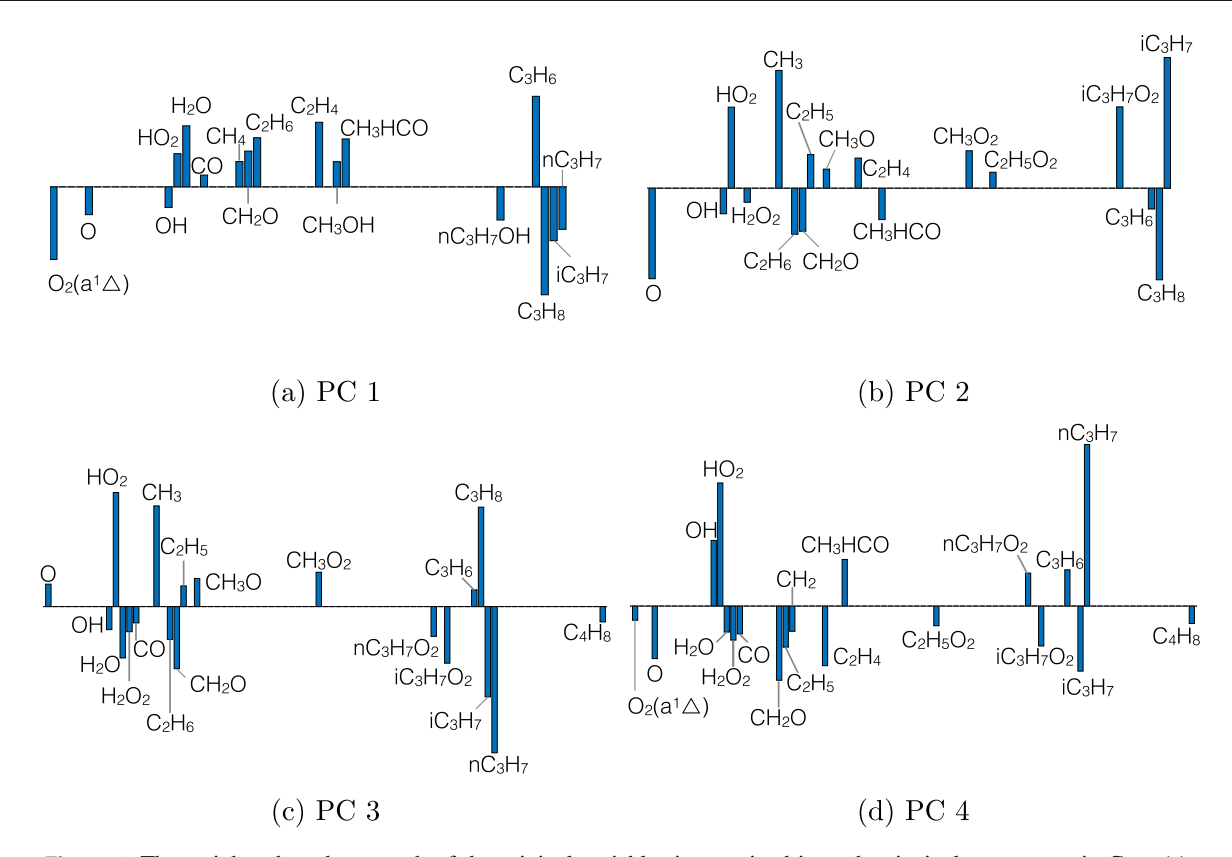


Figure 6. The weights show how much of the original variables is contained in each principal component in Case (a).

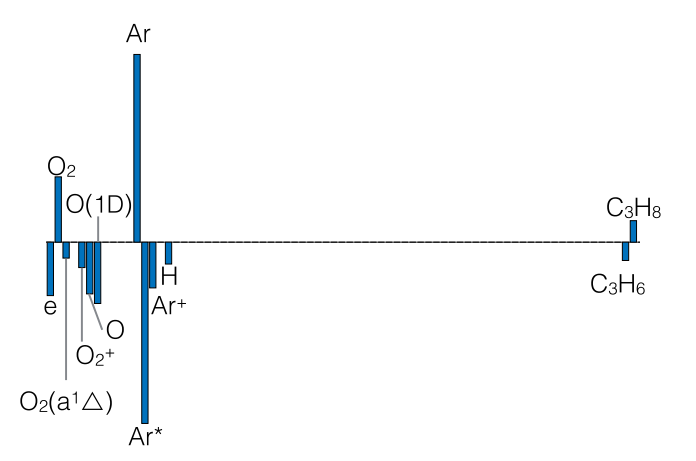


Figure 7. The weighting factors of the first principal component refer to the production of radicals and excited argon and oxygen during the discharge.

using either a single pulse (case (b)) or a burst of identical pulses (case (c)). The power density is 2000 kW cm^{-3} and the pulses are applied at a frequency of 100 kHz with a full-width-half-max (FWHM) of 15 ns. The mixture properties are representative of supersonic combustion and were chosen to obtain practical ignition delay times of the order of $40 \mu s$.

Following the same strategy as for the argon case (Case (a)), PCA is applied on the data from a zero-dimensional reactor simulation employing the detailed fuel-air mechanism.

5.2.1. A priori analysis. Following the same strategy as for the ignition of propane in argon, data were obtained for the

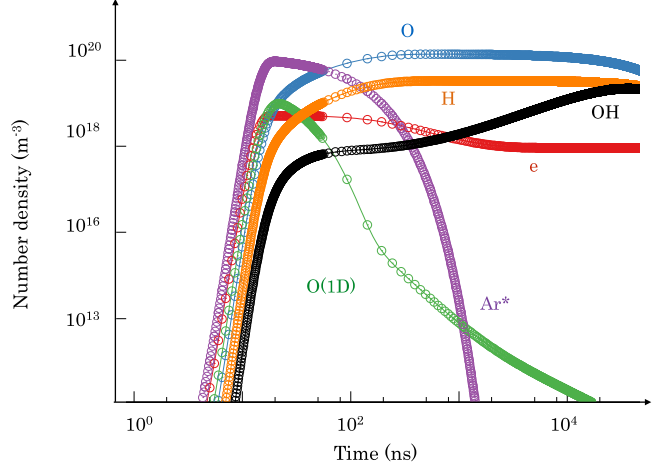


Figure 8. Comparison between the time evolution of the species using the full model (solid lines) and a reduced model with 21 principal components (circles) for Case (a).

ignition of the mixture using a single pulse (case (b)). As part of the preprocessing step, the data were scaled and centered before the PCA. Single centering was used to center the data. This implies that the mean value of each variable is subtracted from each observation. The scree plot in figure 10, representing the value of the normalized eigenvalues for each principal component, indicates the distribution of the variance among the new variables. From the latter it is clear that Pareto scaling performs best as it represents the total variance in the system with less principal components than all

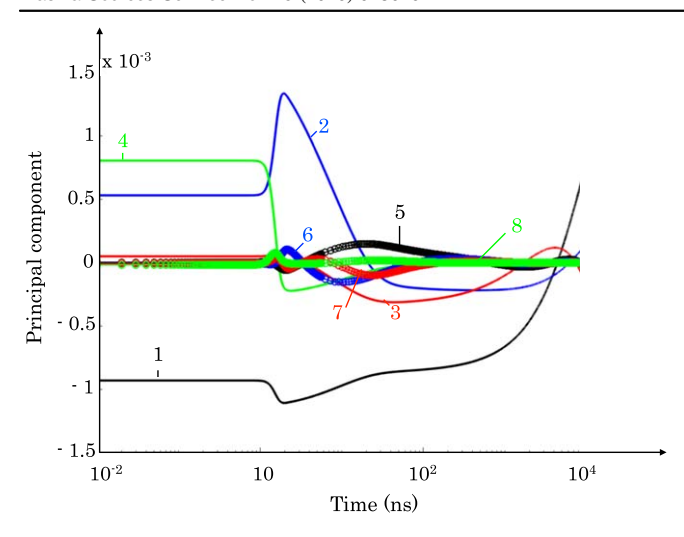


Figure 9. The time evolution of the first 4 principal components in the model with 21 principal components can be related to the dynamics of the system.

Table 3. R^2 value for O, OH, H₂O and H obtained with 40 principal components outside the training conditions in case (a).

T (K)	0	ОН	Н	H ₂ O
650	_	_	_	
750	1	1	1	1
850	0.9997	0.9985	0.9932	0.9995
950	0.9996	0.9961	0.9937	0.9065
1050	0.9991	0.9661	0.9935	0.7272
1150	0.9957	0.8861	0.9872	0.5676
1250	0.9878	0.6083	0.9714	0.4137

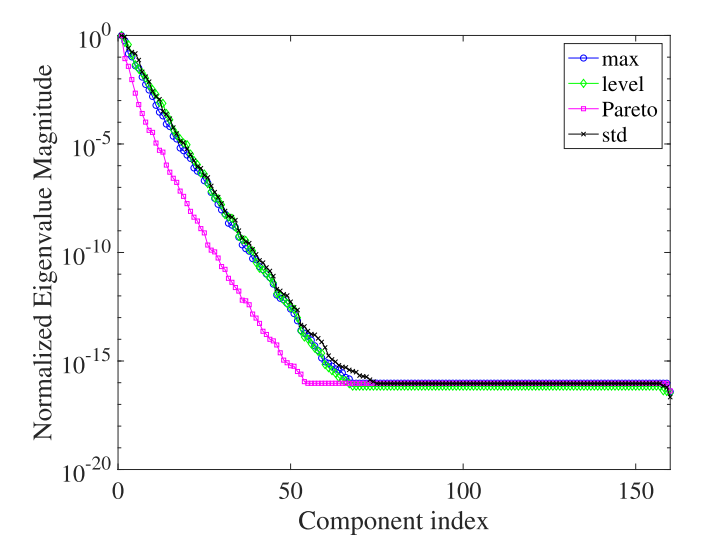


Figure 10. The scree plot shows the normalized eigenvalues against the principal component index for various scaling methods for a single pulse in ethylene/air, Case (b). When using Pareto scaling, the detailed model can be approximated using 50 principal components.

other methods. According to Pareto scaling, 50 principal components are sufficient to describe the dynamics of the full system in the case of a single discharge in air. Figure 11 represents the scree plot for case (c) where a burst of identical

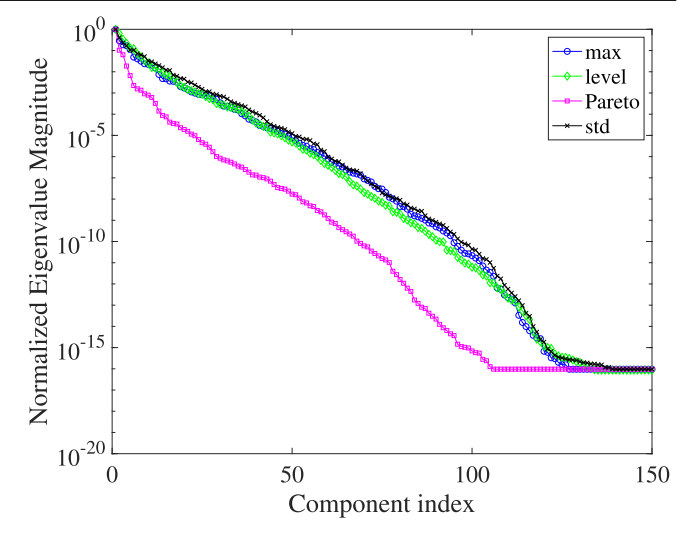


Figure 11. The scree plot shows the normalized eigenvalues against the principal component index for various scaling methods for a burst of pulses in ethylene/air, Case (c). When using Pareto scaling, the detailed model can be approximated using 100 principal components.

pulses is used to ignite ethylene in air. Similarly, the results using Pareto scaling indicate that 100 principal components are needed to represent the full ignition test case. These results are the starting point for developing the reduced mechanism. Recalling the results for argon, the scree plot determined an ideal reduced basis of 25 components. However, the size of the system could be reduced to 21 components as demonstrated with simulations in figure 13. Similar results are expected for the ethylene-air cases.

Figure 12 shows the weights for the first four principal components obtained with the single pulse. The first principal component (figure 12(a)) is representative of the main species in the discharge and shows major contributions of N_2 , O_2 and its first vibrational state $N_2(v1)$. Main combustion species are represented in the second principal component (figure 12(b)) together with $N_2(v1)$ and the oxygen metastable $O_2(a^1\Delta)$. The vibrational levels are well represented in the third principal component (figure 12(c)). The oxygen metastable appears in the fourth principal component together with dominant contributions of HO_2 and H_2O_2 (figure 12(d)).

5.2.2. A posteriori analysis. The a priori analysis has shown that the optimal reduction for a single pulse excitation contains 50 principal components as demonstrated in figure 10. This is taken as the starting point for the generation of a reduced mechanism. After removing additional components, an optimal reduction is reached for 32 principal components in the single pulse test Case (b) as shown in figure 13. The time evolution of the electronically excited states of nitrogen is shown in figure 14. Retaining 32 variables out of 163, corresponds to a model reduction of 80%.

Next, a reduced mechanism was generated for the simulation of the ignition of ethylene using a burst of identical pulses as described in Case (c). The scree plot in

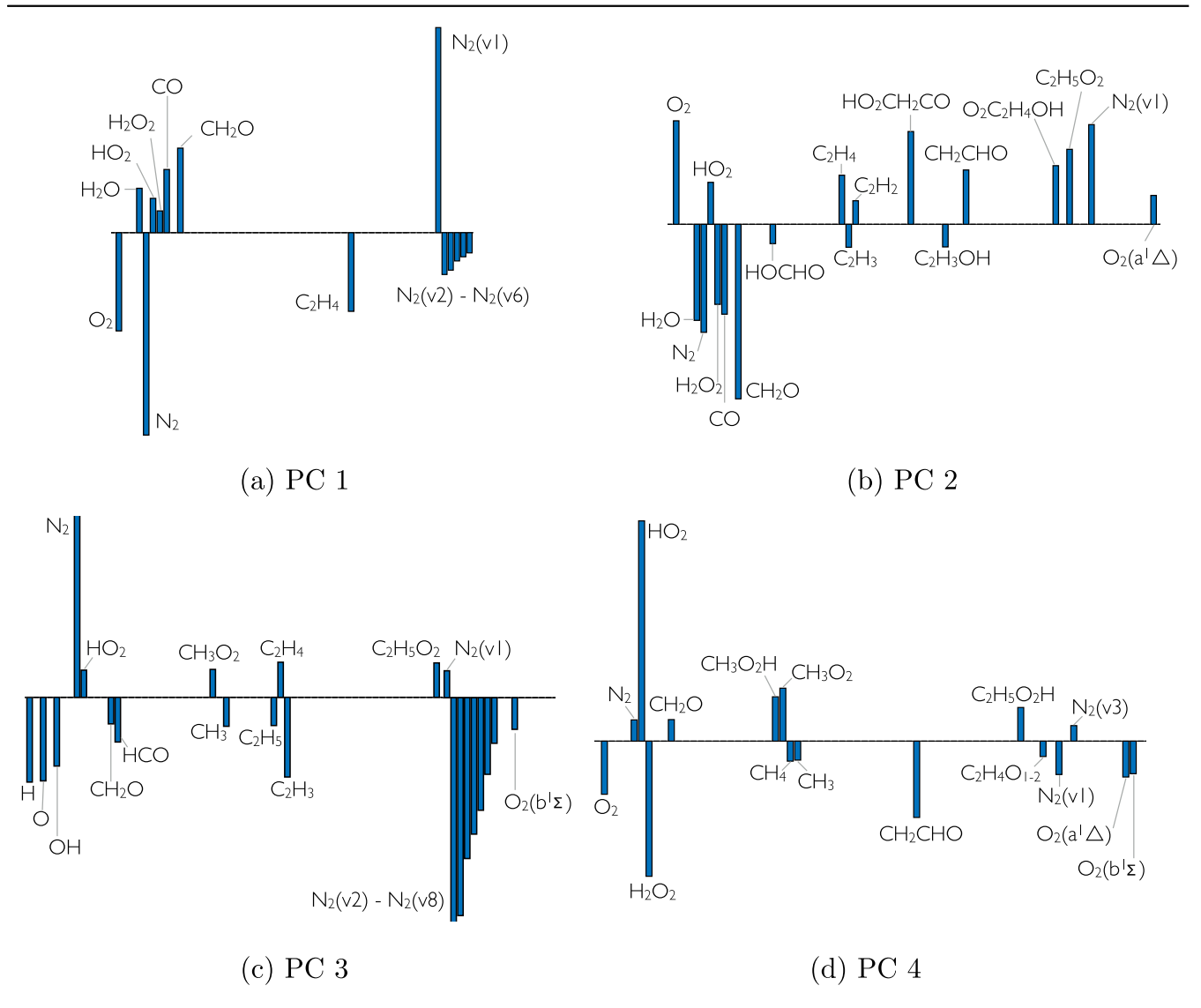


Figure 12. The weights show how much of the original variables is contained in each principal component in Case (b).

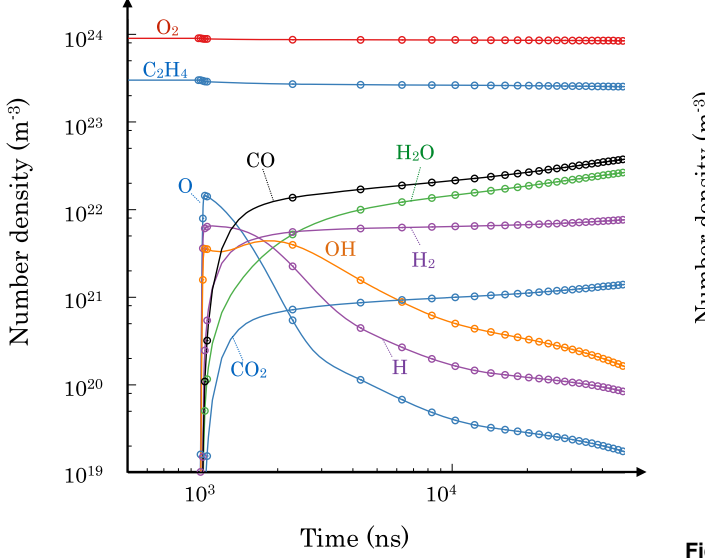


Figure 13. The time evolution of the main species and radicals is shown for the full model (solid lines) against the reduced model with 32 principal components (circles) for Case (b) using a single pulse.

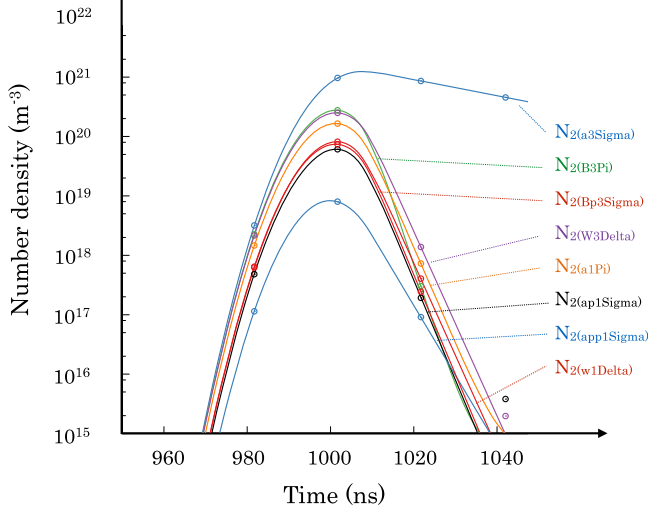


Figure 14. The time evolution of the electronic states of N_2 is shown for the full model (solid lines) against the reduced model with 32 principal components (circles).

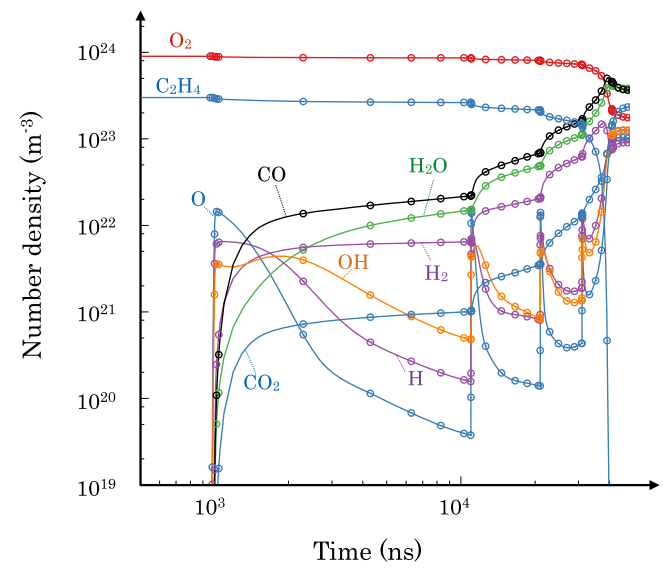


Figure 15. The time evolution of the main species and radicals is shown for the full model (solid lines) against the reduced model with 80 principal components (circles).

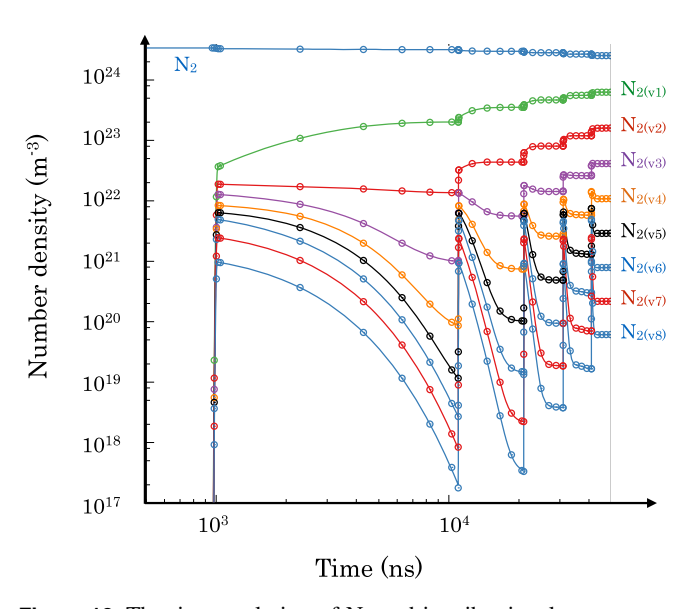


Figure 16. The time evolution of N_2 and its vibrational states $(N_2(v1)-N_2(v8))$ is shown for the full model (solid lines) against the reduced model with 80 principal components (circles).

figure 11 predicted a reduced model using 100 principal components. This number may be optimized to 80 principal components as shown in figure 15. A model reduction of 50% is obtained as only 80 variables are retained out of 163. As the detailed physics of the mechanism is conserved using the optimal amount of principal components, the ignition delay time is identical comparing the full and reduced models (40 μ s). Figures 13 and 15 show a nearly perfect reconstruction of the original state-space. A perfect reconstruction of the number densities of nitrogen and its vibrational and electronic states is shown in figures 16 and 17, respectively. This proves that the plasma dynamics is captured correctly by the reduced model obtained with PCA.

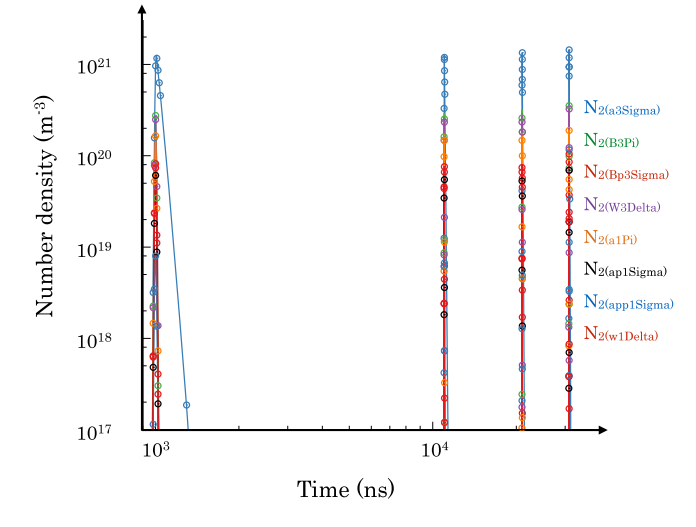


Figure 17. The time evolution of the electronic states of N_2 is shown for the full model (solid lines) against the reduced model with 80 principal components (circles).

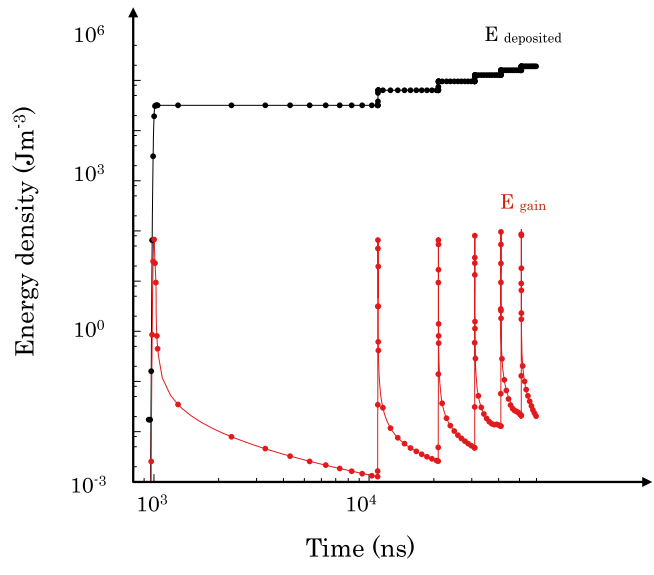


Figure 18. The time evolution of the total deposited energy (black line) and energy gain during each pulse (red line) is shown for the full model (solid lines) against the model with 80 principal components (full circles).

Figure 18 represents the time evolution of the total energy deposited into the mixture and the energy gain during each pulse for both the full model and the reduced model using 80 principal components. The energy is conserved perfectly throughout the ignition simulation using the reduced model. Each single discharge adds additional energy to the gas as can be observed by the step-wise increase of the total deposited energy. The gas temperature is compared in figure 19 and shows excellent agreement. The reduction of 163 species to 80 principal components is satisfying. The dimension of the mechanism is possibly appropriate for two-dimensional unsteady simulations, but possibly too large for three-dimensional ones.

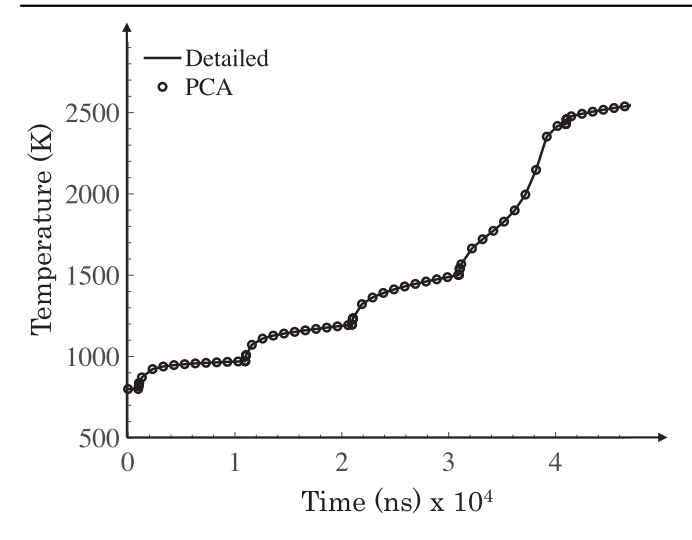


Figure 19. The time evolution of gas temperature is shown for the full model (solid lines) against the model with 80 principal components (full circles).

6. Conclusion

For the first time, PCA is used in order to develop a reduced representation of plasma-enhanced combustion chemistry during nanosecond pulse discharges. The detailed mechanism for a propane-argon mixture containing 103 species and 876 reactions, is reduced to 21 principal components. This corresponds to a dimensionality reduction of approximately 80%. Using the same strategy, the detailed mechanism for a single discharge in ethylene-air is reduced to 32 principal components, reducing the variables by 80%. A model using 80 principal components was developed to simulate the ignition of ethylene in air in conditions representative for supersonic combustion. The new model allows reducing the number of variables by half from 163 species to 80 principal components without introducing any inaccuracies.

The *a priori* investigations presented in this work show that Pareto scaling is the most suitable technique for scaling the data prior to computing the principal components. The new variables in the reduced mechanism, the principal components, relate to the original state-space as they are a linear combination of the primitive variables. By analyzing the contribution of each variable to the principal components, conclusions can be drawn on the key species with regard to radical production and fuel oxidation.

The PCA-models are evaluated *a posteriori* with numerical simulations against data from the full model. Good agreement is obtained for single nanosecond pulse discharge in diluted argon. A model study shows how the reduction based on principal components can be used outside its training conditions. However, the number of components needs to be increased in order to cover reactor conditions outside its training set. The same conclusions can be drawn for the ignition of ethylene in air using a single pulse discharge and a burst of pulses.

Acknowledgments

The research of Aurélie Bellemans was supported by a fellowship of the Belgian American Educational Foundation and the FRS-FNRS. Nicholas Deak and Fabrizio Bisetti were sponsored in part by NSF grant Nr. 1903775.

ORCID iDs

Aurélie Bellemans https://orcid.org/0000-0002-7919-7795

Nicholas Deak https://orcid.org/0000-0003-1543-9334 Fabrizio Bisetti https://orcid.org/0000-0001-5162-7805

References

- [1] Starikovskii A Y, Anikin N B, Kosarev I N, Mintoussov E I, Nudnova M M, Rakitin A E, Roupassov D V, Starikovskaia S M and Zhukov V P 2008 Nanosecondpulsed discharges for plasma-assisted combustion and aerodynamics J. Propul. Power 24 1182–97
- [2] Starikovskaia S M 2014 Plasma-assisted ignition and combustion: nanosecond discharges and development of kinetic mechanisms J. Phys. D: Appl. Phys. 47 353001
- [3] Ju Y and Sun W 2015 Plasma assisted combustion: dynamics and chemistry *Prog. Energy Combust. Sci.* 48 21–83
- [4] Bozhenkov S A, Starikovskaia S M and Starikovskiia A 2003 Nanosecond gas discharge ignition of H₂- and CH₄containing mixtures *Combust. Flame* 133 133–46
- [5] Pancheshnyi S V, Lacoste D A, Bourdon A and Laux C O 2006 Ignition of propane-air mixtures by a repetitively pulsed nanosecond discharge *Trans. Plasma Sci.* 34 2478–87
- [6] Starikovskaia S M 2006 Plasma assisted ignition and combustion J. Phys. D: Appl. Phys. 39 265
- [7] Mintoussov E I, Pendleton S J, Gerbault F G, Popov N A and Starikovskaia S M 2011 Fast gas heating in nitrogen-oxygen discharge plasma: II. energy exchange in the afterglow of a volume nanosecond discharge at moderate pressures J. Phys. D: Appl. Phys. 44 285202
- [8] Tholin F, Lacoste D A and Bourdon A 2014 Influence of fast-heating processes and O atom production by a nanosecond spark discharge on the ignition of a lean H₂-air premixed flame Combust. Flame 161 1235–46
- [9] Adamovich I V, Choi I, Jiang N, Kim J H, Keshav S, Lempert W R, Mintusov E, Nishihara M, Samimy M and Uddi M 2009 Plasma assisted ignition and high-speed flow control: non-thermal and thermal effects *Plasma Sources Sci. Technol.* 18 034018
- [10] Tsolas N, Yetter R A and Adamovich I V 2017 Kinetics of plasma assisted pyrolysis and oxidation of ethylene: II. Kinetic modeling studies *Combust. Flame* 176 462–78
- [11] Starikovskaia S M, Starikovskii A Y and Zatsepin D V 2001 Hydrogen oxidation in a stoichiometric hydrogen-air mixture in the fast ionization wave *Combust. Theor. Model.* 5 97–129
- [12] Aleksandrov N L, Kindysheva S V, Kosarev I N, Starikovskaia S M and Starikovskii A Y 2009 Mechanism of ignition by non-equilibrium plasma *Proc. Combust. Inst.* 32 205–12
- [13] Petrovic Z L, Dujko S, Maric D and Malovic G 2009 Measurement and interpretation of swarm parameters and

- their application in plasma modelling *J. Phys. D: Appl. Phys.* **42** 194002
- [14] Adamovich I V, Li T and Lempert W R 2015 Kinetic mechanism of molecular energy transfer and chemical reactions in low-temperature air-fuel plasmas *Phil. Trans. R.* Soc. A 373 20140336
- [15] Eckert Z, Tsolas N, Togai K, Cherhukho A, Yetter R and Adamovich I V 2018 Kinetics of plasma-assisted oxidation of highly diluted hydrocarbon mixtures excited by a repetitive nanosecond pulse discharge *J. Phys. D: Appl. Phys.* 51 374002
- [16] Togai K, Tsolas N and Yetter R A 2016 Kinetic modeling and sensitivity analysis of plasma-assisted oxidation in a H₂/O₂/Ar mixture *Combust. Flame* 164 239–49
- [17] Lefkowitz J K, Uddi M, Windom B C, Lou G and Ju Y 2015 In situ species diagnostics and kinetic study of plasma activated ethylene dissociation and oxidation in a low temperature flow reactor *Proc. Combust. Inst.* 35 3505–12
- [18] Lefkowitz J K, Guo P, Rousso A and Ju Y 2015 Species and temperature measurements of methane oxidation in a nanosecond repetitively pulsed discharge *Phil. Trans. R. Soc.* A 373 20140333
- [19] Kim W, Mungal M G and Cappelli M A 2008 Formation and role of cool flames in plasma-assisted premixed combustion Appl. Phys. Lett. 92 051503
- [20] Uddi M, Jiang N, Adamovich I V and Lempert W R 2009 Nitric oxide density measurements in air and air/fuel nanosecond pulse discharges by laser induced fluorescence J. Phys. D: Appl. Phys. 42 075205
- [21] Bak M S, Do H, Mungal M G and Cappelli M A 2012 Plasmaassisted stabilization of laminar premixed methane/air flames around the lean flammability limit *Combust. Flame* 159 3128–37
- [22] Yang S, Nagaraja S, Sun W and Yang V 2017 Multiscale modeling and general theory of non-equilibrium plasmaassisted ignition and combustion *J. Phys. D: Appl. Phys.* 50 433001
- [23] Casey T A, Han J, Belhi M, Arias P G, Bisetti F, Im H G and Chen J-Y 2017 Simulations of planar non-thermal plasma assisted ignition at atmospheric pressure *Proc. Combust. Inst.* 36 4155–63
- [24] DeFilippo A C and Chen J-Y 2016 Modeling plasma-assisted methane-air ignition using pre-calculated electron impact reaction rates *Combust. Flame* 172 38–48
- [25] Castela M, Fiorina B, Coussement A, Gicquel O, Darabiha N and Laux C O 2016 Modelling the impact of non-equilibrium discharges on reactive mixtures for simulations of plasma-assisted ignition in turbulent flows Combust. Flame 166 133–47
- [26] Keck J C and Gillespie D 1971 Rate-controlled partialequilibrium method for treating reacting gas mixtures Combust. Flame 17 237–41
- [27] Lu T and Law C K 2005 A directed relation graph method for mechanism reduction *Proc. Combust. Inst.* 30 1333–41
- [28] Ranzi E, Dente M, Goldaniga A, Bozzano G and Faravelli T 2001 Lumping procedures in detailed kinetic modeling of gasification, pyrolysis, partial oxidation and combustion of hydrocarbon mixtures *Prog. Energy Combust. Sci.* 27 99–139
- [29] Pepiot-Desjardins P and Pitsch H 2008 An automatic chemical lumping method for the reduction of large chemical kinetic mechanisms *Combust. Theor. Model.* 12 1089–108
- [30] Munafo A, Panesi M, Jaffe R L, Colonna G, Bourdon A and Magin T E 2012 QCT-based vibrational collisional models

- applied to nonequilibrium nozzle flows *Eur. Phys. J.* D **66** 188
- [31] Jolliffe I 2011 Principal component analysis *International Encyclopedia of Statistical Science* (Berlin: Springer) pp 1094–6
- [32] Coussement A, Gicquel O and Parente A 2013 MG-local-PCA method for reduced order combustion modeling *Proc*. *Combust. Inst.* 34 1117–23
- [33] Isaac B J, Coussement A, Gicquel O, Smith P J and Parente A 2014 Reduced-order PCA models for chemical reacting flows Combust. Flame 161 2785–800
- [34] Malik M R, Isaac B J, Coussement A, Smith P J and Parente A 2018 Principal component analysis coupled with nonlinear regression for chemistry reduction *Combust. Flame* 187 30–41
- [35] Aversano G, Bellemans A, Li Z, Coussement A, Gicquel O and Parente A 2019 Application of reduced-order models based on PCA and Kriging for the development of digital twins of reacting flow applications *Comput. Chem. Eng.* 121 422–41
- [36] Peerenboom K, Parente A, Kozak T, Bogaerts A and Degrez G 2015 Dimension reduction of non-equilibrium plasma kinetic models using principal component analysis *Plasma* Sources Sci. Technol. 24 025004
- [37] Bellemans A, Munafo A, Magin T E, Degrez G and Parente A 2015 Reduction of a collisional-radiative mechanism for argon plasma based on principal component analysis *Phys. Plasma* 22 062108
- [38] Bellemans A, Magin T E, Coussement A and Parente A 2017 Reduced-order kinetic plasma models using principal component analysis: model formulation and manifold sensitivity *Phys. Rev. Fluids* 2 073201
- [39] Bellemans A, Parente A and Magin T E 2018 Principal component analysis acceleration of rovibrational coarsegrain models for internal energy excitation and dissociation J. Chem. Phys. 148 164107
- [40] Cohen S D, Hindmarsh A C and Dubois P F 1996 CVODE, a Stiff/Nonstiff ODE solver in C Comput. Phys. 10 138–43
- [41] Piper L G, Velazco J E and Setser D W 1973 Quenching cross sections for electronic energy transfer reactions between metastable argon atoms and noble gases and small molecules *J. Chem. Phys.* **59** 3323–40
- [42] Jauberteau J L, Thomas L, Aubreton J, Jauberteau I and Catherinot A 1998 High reactivity of CH₂ radical in an Ar-CH₄ post-discharge *Plasma Chem. Plasma Process.* 18 137-51
- [43] Hagelaar G J M and Pitchford L C 2005 Solving the Boltzmann equation to obtain electron transport coefficients and rate coefficients for fluid models *Plasma Sources Sci. Technol.* 14 722
- [44] Pitchford L C et al 2017 LxCat: an open-access, web-based platform for data needed for modeling low temperature plasmas Plasma Process. Polym. 14 1600098
- [45] Parente A and Sutherland J C 2013 Principal component analysis of turbulent combustion data: data pre-processing and manifold sensitivity *Combust. Flame* 160 340–50
- [46] Bellemans A, Aversano G, Coussement A and Parente A 2018 Feature extraction and reduced-order modelling of nitrogen plasma models using principal component analysis *Comput. Chem. Eng.* 115 504–14
- [47] Xiang S, Nie F and Zhang C 2008 Learning a mahalanobis distance metric for data clustering and classification *Pattern Recognit* 41 3600–12
- [48] Franklin R N 2002 The role of the $O_2(a^1\Delta_g)$ metastable in oxygen discharges *J. Phys. D: Appl. Phys.* **35** 1094